Applied Catalysis B: Environmental 186 (2016) 127–135

Contents lists available at ScienceDirect

Applied Catalysis B: Environmental

journal homepage: www.elsevier.com/locate/apcatb

Ultrasmall graphitic carbon nitride quantum dots decorated self-organized TiO_2 nanotube arrays with highly efficient photoelectrochemical activity

Jingyang Su [a], Lin Zhu [b], Guohua Chen [a,b,c,*]

[a] Environmental Engineering Program, School of Engineering, The Hong Kong University of Science and Technology, Clear Water Bay, Kowloon, Hong Kong, China
[b] Fok Ying Tung Graduate School, The Hong Kong University of Science and Technology, Clear Water Bay, Kowloon, Hong Kong, China
[c] Department of Chemical and Biomolecular Engineering, The Hong Kong University of Science and Technology, Clear Water Bay, Kowloon, Hong Kong, China

ARTICLE INFO

Article history:
Received 11 October 2015
Received in revised form
14 December 2015
Accepted 30 December 2015
Available online 6 January 2016

Keywords:
Graphitic carbon nitride
TiO_2
Quantum dots
Photoelectrochemical activity
Pollution control
Water splitting

ABSTRACT

In the present study, a novel graphitic carbon nitride quantum dots (CNQDs) modified TiO_2 nanotube arrays (NTAs) photoelectrode was successfully synthesized by a simple two-step method which includes an electrochemical anodization technique followed by a facile organic molecular linkage. The successful modification of TiO_2 by CNQDs was found to improve the photoelectrochemical activity significantly because of enhanced light absorption and improved separation of photo-generated electron–hole pairs. The optimized CNQDs/TiO_2 NTAs showed nearly 3.5-fold photocurrent of that from TiO_2 NTAs alone at 0.3 V vs Ag/AgCl and the maximum photoconversion efficiency reaches up to 0.63% in neutral solution under simulated solar light irradiation. Furthermore, the prepared CNQD/TiO_2 NTAs demonstrated superior photoelectrocatalytic activity and stability in the degradation of RhB, with kinetic constants 3.0 times of that from TiO_2 NTAs. The hydroxyl and superoxide radicals were proved to be the dominant active radicals during pollutants degradation. Additionally, the prepared CNQD/TiO_2 sample was used as photoanodes for direct photoelectrochemical water splitting to produce H_2 and O_2 under simulated solar light illumination, achieving a H_2 production rate with 22.0 μmol h^{-1} cm^{-2} at 0.3 V vs Ag/AgCl.

1. Introduction

Efficient solar energy utilization and conversion for storable clean fuels is one of promising strategies for production of renewable energy source in sustainable development. Photocatalysis using earth abundant elements is one of the advanced physicochemical processes applied in the organic pollutants degradation and water splitting for hydrogen production [1–7]. Among various photocatalysts, TiO_2 remains the most commonly used semiconductor for photocatalytic degradation of wide range organic pollutants and water splitting due to its high surface area, excellent stability and efficient charge transfer [5,8–10]. Recently, vertically oriented TiO_2 nanotube arrays (NTAs) have attracted much interest, which were prepared through an electrochemical anodization process with highly ordered surface morphology and improved photoelectrochemical (PEC) activity compared with traditional TiO_2 nanofilm [10–14]. However, the applications of TiO_2 NTAs are still limited by its wide band gap that is only photo-responsive under UV illumination. Since UV illumination accounts for only 5% of the solar spectrum, even though the quantum efficiency of TiO_2 NTAs exceeds 80% [15], the solar photo-conversion efficiency is still low compared with smaller band-gap semiconductors. Therefore, red shifts of absorption band from UV towards visible light region, which accounts for 45% of the whole solar spectrum, will increase the visible light utilization of TiO_2 NTAs and further photoconversion efficiency. During the past decade, a variety of strategies have been employed to resolve the issue and modify electronic structures of TiO_2 to narrow down the band gap, for example, via suitable textural design, doping with nonmetal or metal [16–19], sensitization to form a heterojunction by combining TiO_2 with metal or other semiconductors [20–24]. Among these, the construction of a semiconductor heterojunction has attracted great attention due to its perfect effectiveness in improving the PEC activity. Comparing with other sensitizers, semiconductor quantum dots (QDs) with tunable absorption band edge by varying the size of QDs

* Corresponding author at: Department of Chemical and Biomolecular Engineering, The Hong Kong University of Science and Technology, Clear Water Bay, Kowloon, Hong Kong, China.
E-mail address: kechengh@ust.hk (G. Chen).

http://dx.doi.org/10.1016/j.apcatb.2015.12.050
0926-3373/

offer new opportunities to harvest light energy in the visible light region. Various QDs as visible light absorber to modify TiO_2 NTAs with improved photoelectrochemical activity have been investigated, such as CdS [25,26], CdSe [27], CdTe [28], PbS [29] and ZnS [30]. However, these QDs may induce serious health and environmental problems due to the involvement of toxic metals, which limits their wide applications.

Graphitic carbon nitride (CN) is a newly developed metal free semiconductor with band gap of 2.7 eV and excellent biocompatibility [31,32], which has been widely explored in photocatalytic hydrogen evolution [31–34], pollutants degradation [35,36], oxygen reduction reaction [37,38] and bioimaging [39]. Recently, graphitic carbon nitride quantum dots (CNQDs) were synthesized with narrow size distribution and high fluoresence through a simple solid thermal reaction [40]. It is promising to combine CNQDs with TiO_2 NTAs to constitute a heterostructure, since both the utilization of visible light and the surface-interface charge transfer efficiency of photo-generated carriers could be improved. Hence, we report highly ordered TiO_2 NTAs decorated with CNQDs through a delicate bifunctional organic molecule as an effective linker. The photoelectrocatalytic activity of the CNQDs/TiO_2 NTAs heterostructure was evaluated by degrading rhodamine B (RhB). Furthermore, direct water splitting to produce hydrogen and oxygen gas in aqueous solution using prepared photoanodes was explored as well.

2. Experimental

2.1. Preparation of CNQDs/TiO_2 NTAs photoelectrodes

The fluorescent CNQDs were synthesized by a low-temperature solid-phase method with urea and sodium citrate as the precursors, which are reported in the previous study [40]. In details, the solid mixtures of urea and sodium citrate with a molar ratio of 6:1 were thermally treated under 180 °C in an autoclave for 2 h. Then the produced CNQDs were extracted from the resultant yellowish powders by washing with alcohol and subsequent dialyzing against pure water for 24 h using dialysis membrane (MWCO 3500, Spectra/Por). Through the dialysis process, the reactants left in the final products could be removed to water and get purified.

TiO_2 NTAs were fabricated by a two-step anodization process. Prior to anodization, the Ti foils were first degreased by sonicating in acetone, ethanol and DI water, respectively, followed by drying in dry air stream for 30 min. The anodization process was carried out in a conventional two-electrode system with the Ti foil as the anode and a Pt foil as the cathode. The electrolyte consisted of 0.5 wt% NH_4F and 2 vol% water in ethylene glycol (EG) solution. All the anodization process was carried out at room temperature of 25 °C. In the first-step anodization, the Ti foil was anodized at 60 V for 60 min, and then the as-grown nanotubes layer was ultrasonically removed in 1 M HCl solution. The produced Ti foil then underwent the second anodization at 60 V for 30 min, producing a nanoring-nanotube structure. After the two-step anodization, the prepared TiO_2 NTAs samples were cleaned with DI water and dried with nitrogen gas for 30 min. Then the anodized TiO_2 NTAs samples were annealed in air at 450 °C for 2 h with a heating rate of 2 °C min^{-1} for phase conversion from amorphous to crystalline. As TiO_2 has a strong affinity for the carboxylate group of the linker molecules, bifunctional linker molecules 3-mercaptopropionic acid (MPA) with carboxylate and thiol functional groups was used to facilitate the binding of CNQDs to TiO_2 [27,41]. The annealed TiO_2 NTAs were immersed in a 10 mg mL^{-1} of CNQDs aqueous solution at 80 °C for 12 h together with 1 v% MPA solution. The resulting TiO_2 NTAs were washed with deionized water and dried in air for 30 min.

2.2. Characterization

Surface morphologies of TiO_2 NTAs and CNQDs/TiO_2 NTAs were examined by Field Emission Scanning Electron Microscopy (FESEM, JEOL 7100F). The structure and shape of the CNQDs and CNQDs/TiO_2 NTAs were also examined by a High Resolution Transmission Electron Microscope (HRTEM, JEOL JEM2010F), equipped with an Electron Energy Loss Spectroscopy (EELS). X-ray Photoelectron Spectroscopy (XPS) was recorded on a PHI 5600 (Physical Electronic, USA) equipped with an Al monochromatic X-ray source. C 1s line at 284.6 eV was used as the calibration reference before each measurement. Fourier Transform Infrared Spectra (FT-IR) were recorded on a VERTEX 70-FTIR with the standard KBr pellet method. Photoluminescence spectra (PL) were measured at room temperature of 25 °C on a Shimadzu RF-5301 PC spectrometer using a 325 nm excitation light.

2.3. Photoelectrochemical measurement

PEC measurements were performed using a conventional three-electrode cell system and an electrochemical workstation (PGSTAT 100, Autolab, Netherlands). The prepared electrode was employed as the working electrode. Meanwhile, a saturated Ag/AgCl electrode and a platinum electrode served as the reference and counter electrode, respectively. All the potentials were referred to the saturated Ag/AgCl unless otherwise stated. Some 0.1 M Na_2SO_4 (pH 6.0) was the electrolyte. A 300 W high-pressure xenon short arc lamp (Newport) was used as the simulated solar light source to provide a light intensity of 100 mW cm^{-2}, which was calibrated prior to every photoelectrochemical test using a calibrated Si photodiode. Linear sweep voltammetry curves were measured at a scanning rate of 20 mV s^{-1}, ranging from −0.5 V to 1.0 V vs Ag/AgCl. Electrochemical impedance spectroscopy (EIS) was carried out in the frequency range of 0.01–10^5 Hz with an AC voltage amplitude of 5 mV at a bias of 0 V (vs Ag/AgCl) in 0.1 M Na_2SO_4 solution.

2.4. Photoelectrochemical performance test

The photoelectrocatalytic activities of the prepared TiO_2 NTAs and CNQDs/TiO_2 NTAs were investigated by degrading RhB as model pollutant in aqueous solution. The initial concentration of RhB is 10 mg L^{-1}. The concentration change of RhB during degradation was examined by measuring the maximal absorption at λ = 554 nm using an UV–vis spectrophotometer (Unico UV-2012PC, USA). Total organic carbon (TOC) was measured using a TOC analyzer (TOC-V_{CPH}, Shimadzu, Japan). The reactive oxygen species $^{\bullet}OH$ and $^{\bullet}O_2^-$ were detected using a Bruker Elexsys A200 electron spin resonance spectrometer (ESR, Bruker, Germany) with a 100 W short arc mercury lamp (ER 203UV system) as the irradiation light source. Photoelectrochemical water splitting reaction for hydrogen and oxygen production was conducted in a three electrode system where the reaction vessel was connected to a glass-closed gas-circulation system. The water splitting experiment was carried in a sealed quartz cell containing 0.1 M Na_2SO_4 electrolyte (pH 6.0) under vacuum conditions at 0.3 V vs Ag/AgCl. The reaction solution was maintained at 25 °C using a flow of cooling water during the reaction. The evolved gases were analyzed using a gas chromatograph equipped with a thermal conductive detector.

3. Results and discussion

A high resolution TEM image of CNQDs is shown in Fig. 1A, demonstrating that the prepared CNQDs are mono-dispersed in water solution and uniform in size of each quantum dot. According to the HRTEM image, an average diameter of prepared CNQDs 5.0 nm is obtained. Moreover, the core-level EELS spectrum of the

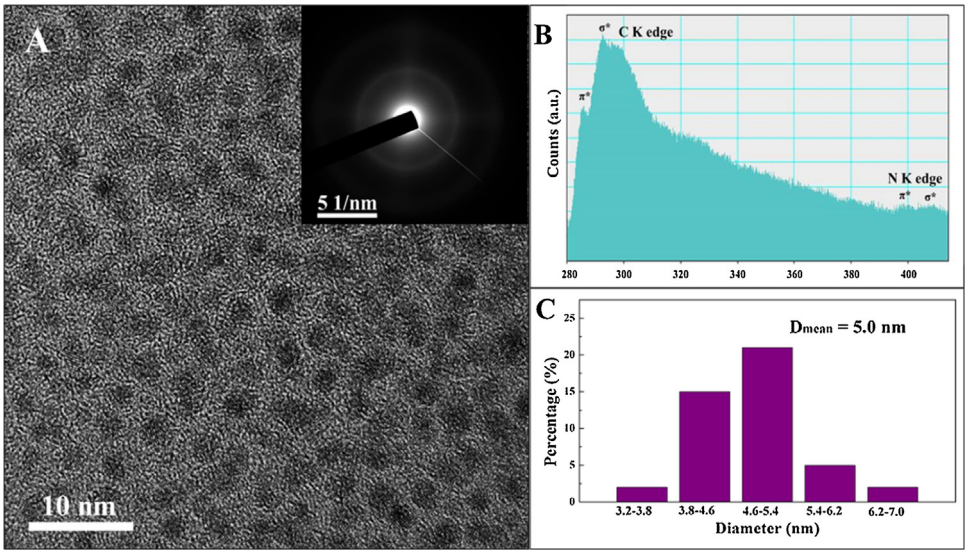

Fig. 1. TEM images (A, inset is SAED spectrum), EELS (B) and size distribution (C) of prepared CNQDs.

CNQDs (Fig. 1B) shows that the system is exclusively composed of sp^2-hybridized carbon and nitrogen atoms, as indicated by the presence of the 1 s/p* transition for both elements [42,43]. The carbon-K ionization edge and nitrogen-K ionization edge show identical near edge structures indicating a similar threefold coordination and electronic environment of the carbon and nitrogen in the synthesized material.

The remarkable optical properties of the as-obtained CNQDs are confirmed by the UV–vis absorption and the PL spectra. As shown in Fig. S1 (black curve), UV–vis spectrum indicates a characteristic absorption peak at 344 nm for the CNQDs. The narrow and symmetrical fluorescence spectra (red curve) show that the emission peak is 442 nm at the excitation wavelength of 325 nm, which demonstrating a blue shift ~20 nm compared with the bulk g-C_3N_4 (~462 nm) [39]. The blue shift of PL spectra can be ascribed to the quantum confinement effect with the conduction and valence band shifting in opposite directions. The digital picture (Fig. S1 inset) of the aqueous dispersions further shows that the obtained CNQDs are water-soluble and exhibit strong blue fluorescence under 325 nm UV light illumination. Furthermore, The XRD pattern of prepared CNQDs was provided in Fig. S2. Clearly, a strong peak ⟨0 0 2⟩ at 27.2° can be observed, which is corresponding to interlayer d-spacing of 0.33 nm in previous reported graphitic carbon nitride quantum dots [44].

The surface morphology of prepared CNQDs/TiO_2 NTAs was examined by SEM. Fig. 2 shows typical SEM top images of the vertically oriented TiO_2 NTAs and modified TiO_2 NTAs by CNQDs. From Fig. 2A, a regularly arranged nanotube with uniform nano-ring morphology can be observed, and the average diameter is around 110 nm. Through the MPA linking, it is found that surface of the TiO_2 NTAs is covered with dispersed CNQDs aggregated nanoparticles without blocking the channels and a well-ordered nanotube structure still exist after modification process by MPA linking (Fig. 2B), suggesting that the modification process is a facile procedure that does not damage the ordered nanotube structure. The thickness of prepared film is around 5 μm (Fig. 2B inset), which can guarantee enough light absorption both in UV and visible light region.

The morphology of CNQDs modified TiO_2 NTAs were further investigated using TEM and HRTEM. At low magnification of TEM images (Fig. 3A and B) of the prepared sample, an ordered array tubular structure can be observed clearly. Fig. 3C is a TEM image with higher-magnification showing several nanotubes arranged in arrays. It reveals that CNQDs have been successfully deposited onto TiO_2. The observed lattice spacing of 0.35 nm in Fig. 3D corresponds to the (1 0 1) plane of anatase TiO_2. The observed CNQDs are dispersed and visible on the TiO_2 (marked in red circles), and the clear lattice spacing of 0.34 nm can be identified, corresponding to the (0 0 2) plane of hexagonal CN [31,45]. This result is consistent with XRD pattern obtained from pure CNQDs as reported in previous research (see Fig. S2) [44]. Also, TEM-EDX elemental mapping (Fig. S3) gave visible evidence that carbon and nitrogen were homogenously dispersed within the TiO_2 tubular structure.

The XPS survey spectrum (Fig. 4A) of the CNQDs/TiO_2 NTAs also confirmed the existence of Ti, O, C and N elements. The O 1s core level peak at 529.7 eV comes from Ti—O—Ti linkages in TiO_2 (Fig. 4B), which is consistent with that of the previous report [46]. After CNQDs modification, the peak at 531.4 eV belonging to —OH functional groups on the surface of CNQDs can be identified, which is much higher than that of pristine TiO_2 (Fig. S4), revealing the successful decoration of CNQDs onto TiO_2 NTAs. To identify different contributions of the N 1s (Fig. 4C) and C 1s (Fig. 4D) peaks, the spectrum was deconvoluted into various peaks as shown. From the results, the C 1s peak at 284.6 eV is assigned to the C—C bond in the turbostratic CN structure, and the peak at 286.1 eV is attributed to the sp^2C atoms bonded to N inside the aromatic structure. The peak at 288.8 eV is attached to the sp^3 C—N bond of the sp^3 bonded composition. The N 1s peaks are comprised of three components centered at 399.1 eV, 400.1 eV and 401.3 eV, which are identified as the C—N—C, (N—$(C)_3$) and C—N—H groups, respectively. It is notable that the binding energy of C—N—C is a slightly higher than the value reported from layered C_3N_4 (usually 388.5–388.8 eV). The possible reason is there are abundant functional groups with strong electronegativity (hydroxyl, carboxyl etc.) existing on the surface of as-prepared quantum dots. These functional groups can affect electronic cloud distribution of the material, leading to binding energy shift towards higher energy. This phenomenon has been widely observed in carbon nitride quantum dots [44,47] and nitrogen doped carbon quantum dots [48,49]. The presence of the N—$(C)_3$ groups confirms the polymerization of urea in the solid thermal reaction, and the existence of (C—N—H) amino functional groups demonstrates that the synthesis of CNQDs by pyrolysis of urea is incompletely condensed [40,50].

FT-IR analysis is conducted to study the surface chemistry of the prepared samples, and the results of pristine TiO_2, CNQDs and CNQDs/TiO_2 are shown in Fig. S6 (SI). From the spectra, the characteristic breathing mode of triazine units which belongs to graphitic

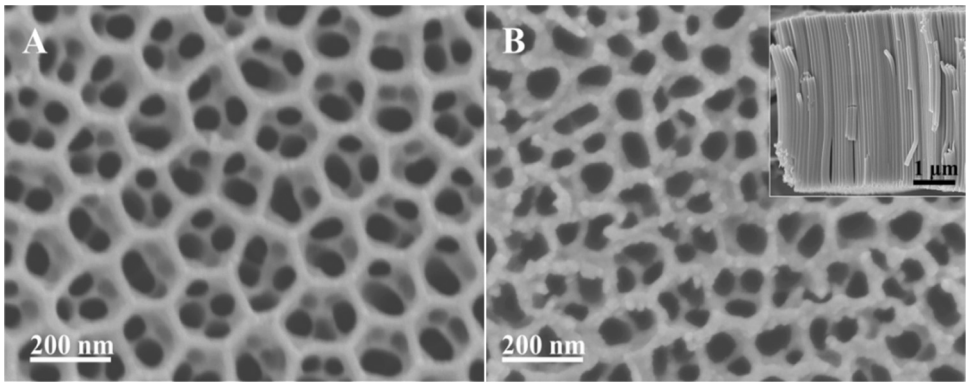

Fig. 2. SEM images of representative TiO_2 NTAs (A) and CNQDs/TiO_2 NTAs (B) (inset is cross-sectional image).

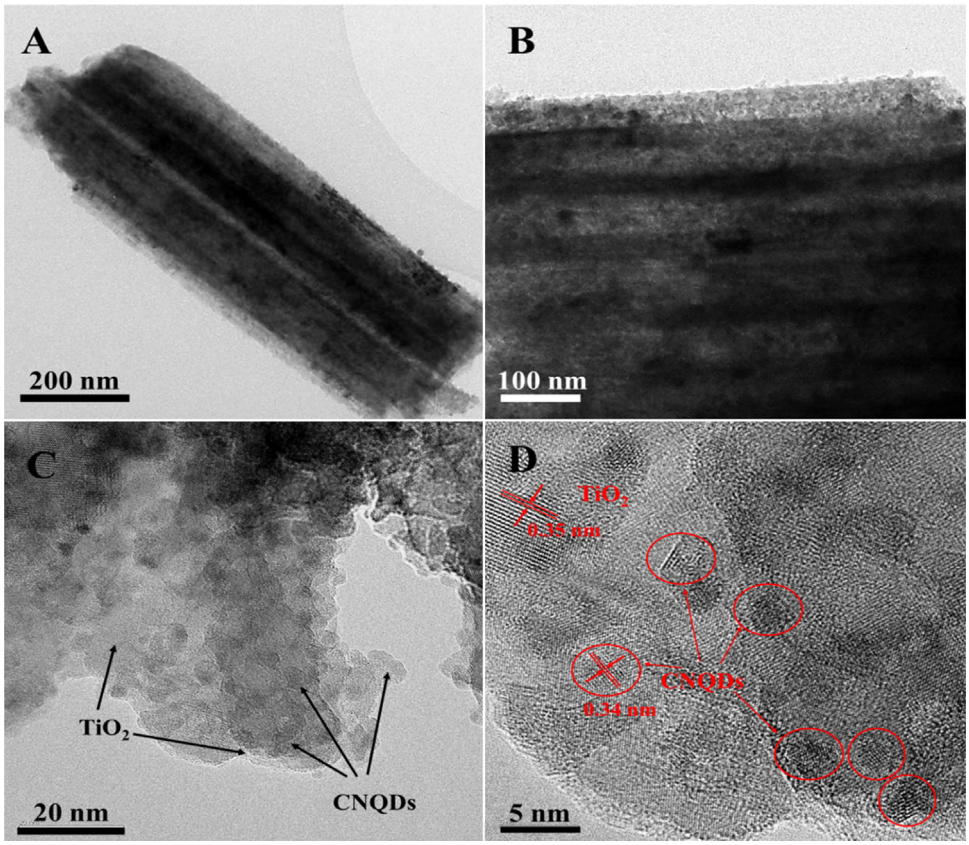

Fig. 3. TEM (A, B) and HRTEM (C, D) images of prepared CNQDs/TiO_2 NTAs.

carbon nitride at 810 cm^{-1} is observed. Several strong bands in the 1200–1600 cm^{-1} region dominate the spectrum, with the peaks at about 1150, 1390, and 1590 cm^{-1}, which correspond to the typical stretching mode of CN heterocycles [45,50]. Additionally, a broad band near 3180 cm^{-1} region can be attributed to the stretching vibration of N—H groups at the defect sites of the aromatic ring [51,52], shown in both CNQDs and CNQDs/TiO_2 NTAs. The result indicates the aromatic rings structure of CNQDs. Moreover, the peaks near 1625 cm^{-1} is considered to be Ti—OH stretching band showing in the pristine TiO_2 NTAs and CNQDs/TiO_2 NTAs sample and 3460 cm^{-1} is in consistent with adsorbed water which is clear in all three curves. Hence, these characteristic peaks prove the existence of CNQDs in the modified TiO_2 NTAs photoelectrode.

Fig. 5A shows the linear sweep voltammetry curves of prepared samples which were carried out under simulated solar light illumination in 0.1 M Na_2SO_4 aqueous solution. Clearly, prepared CNQDs/TiO_2 NTAs exhibit significantly improved photoresponse under light illumination, and the saturation photocurrent reaches 1.34 mA cm^{-2} at 0.3 V vs Ag/AgCl, nearly 3.5 times of pristine TiO_2 (0.38 mA cm^{-2}) at the same condition. The photoconversion efficiency of the CNQDs/TiO_2 photoelectrode achieves up to 0.63% at a low potential of 0.1 V vs Ag/AgCl (Fig. 5B). To the best of our knowledge, it is one of the highest reported values which were tested in neutral solution without buffer. Furthermore, photocurrent densities vs time curve was conducted in the same electrolyte with several 30 s light on/off cycles at 0.3 V vs Ag/AgCl shown in Fig. 5C. The prepared CNQDs/TiO_2 NTAs exhibited excellent photo-stability after 360 s PEC test, achieving a photocurrent higher than 1.3 mA cm^{-2}, whereas pristine TiO_2 NTAs only realized 0.37 mA cm^{-2}, revealing that the electron transfer and separation process is beneficial from the existence of heterojunction structure. It is notable that the obtained photocurrent is higher than carbon

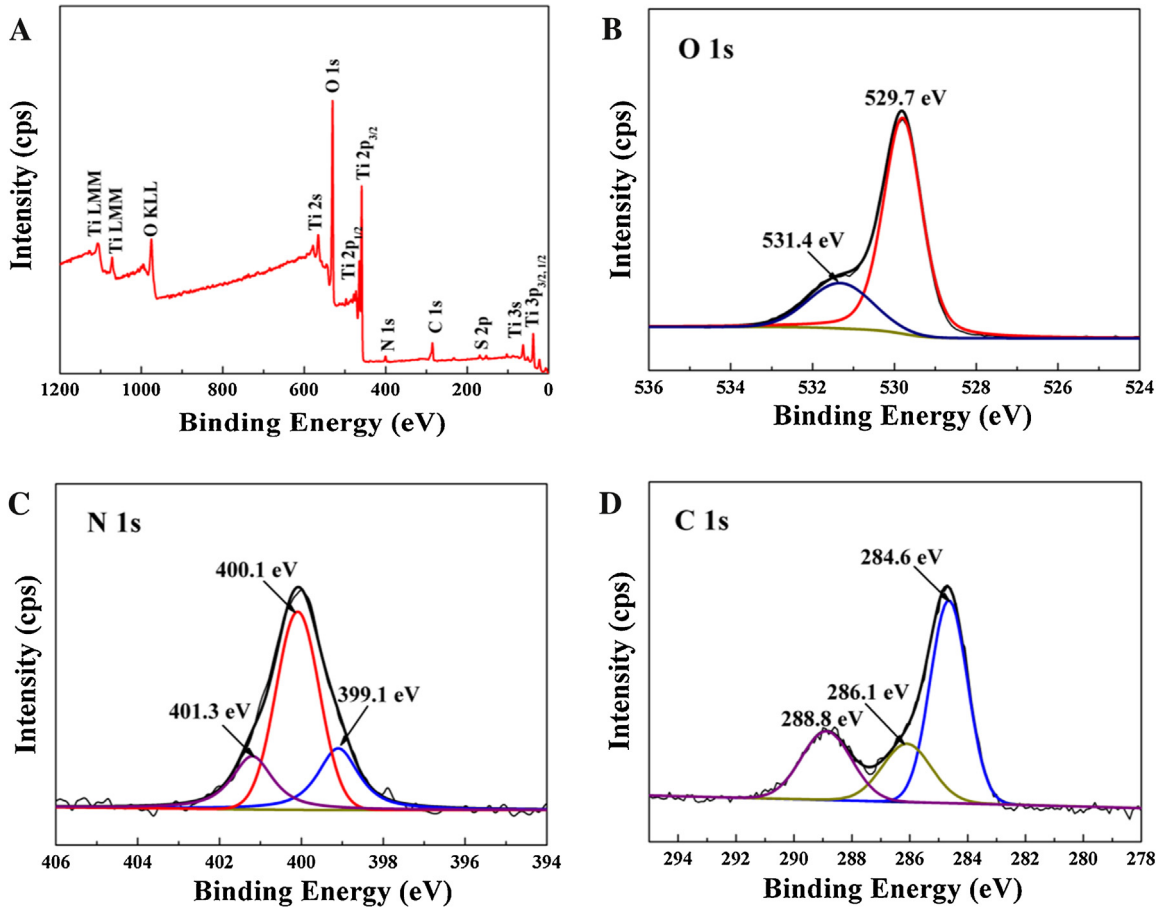

Fig. 4. XPS survey spectrum (A) of and corresponding core level spectra (B) O 1s, (C) N 1s and (D) C 1s of CNQD/TiO_2 NTAs.

quantum dots and other approaches modified TiO_2 NTAs in the previous reports (SI, Table S1), revealing that CNQDs as an efficient sensitizer can improve the PEC performance of formed heterojunction effectively. Besides, measurements of incident photon to current conversion efficiency (IPCE) of prepared photoanodes were tested to study the photoresponse of pristine CNQDs modified TiO_2 NTAs as a function of incident light wavelength (Fig. 5D). Clearly, pristine TiO_2 shows strong photoresponse only in the UV region (300–400 nm). Surprisingly, the modified samples display significantly improved photoactivity in the visible light region from 400 to 500 nm in addition to strong response in the UV region. Particularly, the IPCE of CNQDs/TiO_2 NTAs photoanodes at the monochromatic wavelength of 420 nm is up to 6.8%, while the value is negligible for pristine TiO_2 under same condition. These results demonstrate the much enhanced visible light utilization contributes higher PEC response. Moreover, the performance of TiO_2 and CNQDs/TiO_2 NTAs was tested under visible light irradiation ($\lambda > 420$ nm). As can be seen from Fig. S7, the prepared CNQDs/TiO_2 shows significantly enhanced visible light activity than pure TiO_2: nearly 0.06 mA cm^{-2} photocurrent density can be achieved on CNQDs/TiO_2 NTAs, while the photo-response of pristine TiO_2 NTAs is negligible. This result reveals that CNQDs can be excited by visible light, resulting in enhanced visible light photocurrent of CNQDs/TiO_2 heterojunction.

The high IPCE of CNQDs/TiO_2 both in UV and visible light region can further be verified by UV–vis absorption spectra (Fig. 6A). As one can see, for pristine TiO_2, it can only absorb light with wavelength shorter than 390 nm, with the band gap around 3.2 eV. However, after CNQDs modification, the produced sample shows much enhanced light absorption ranging from 300 nm to 500 nm. These results provide a direct evidence for the enhanced light absorption which is resulted from the photosensitization of CNQDs. Moreover, the separation and transfer of electron and hole pairs can be analyzed using EIS. The semicircle in the Nyquist plots in EIS tests conveys information on the charge transfer process with the diameter of the semicircle corresponding to the charge transfer resistance. Fig. 6B shows the Nyquist plots of TiO_2 NTAs and CNQDs/TiO_2 NTAs electrodes under light and dark conditions, respectively. Among them, CNQDs/TiO_2 NTAs under light illumination shows the smallest semicircular diameter compared with other counterparts. This result indicates that CNQDs/TiO_2 NTAs possess a smaller charge transfer resistance than that of pristine TiO_2 NTAs, suggesting improved charge separation efficiency.

To further investigate the PEC activity of the CNQDs/TiO_2 NTAs, RhB degradation experiments were carried out under simulated solar light irradiation. The RhB removals in the various degradation processes, including the dark control, electrochemical, photolytic, photocatalytic and PEC process are presented in Fig. 7A. It is obvious that the PEC process provides the most powerful approach to degrade the RhB in aqueous solution, and nearly 100% RhB was removed over 90 min in PEC process (Fig. S8). The 39% of RhB removal was obtained after 90 min in photocatalytic process, while only 11% of the RhB removal was obtained in photolytic process with the same illumination time. The removal efficiency in electrochemical process was insignificant due to the negligible current of CNQDs/TiO_2 NTAs under the dark. Additionally, the degradation of RhB in the PEC process was much higher than the summation of the individual photocatalytic and electrochemical processes. Obviously, a synergetic effect was observed on the CNQDs/TiO_2 NTAs during PEC degradation. Furthermore, RhB degradation by CNQDs electrode and TiO_2 NTAs was evaluated in PEC process for

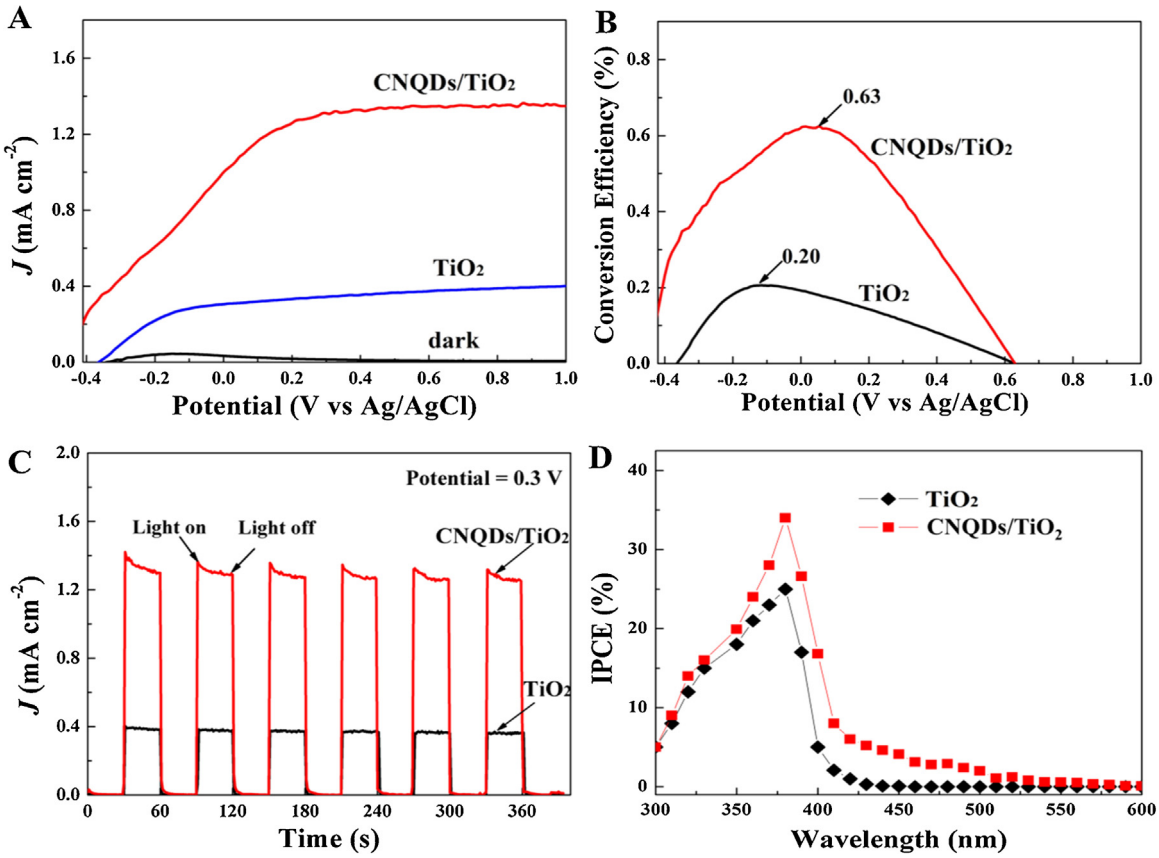

Fig. 5. (A) photocurrent densities versus voltage curves, (B) corresponding photoconversion efficiency, (C) photocurrent densities versus time curves and (D) measured IPCE spectra of TiO_2 and CNQDs/TiO_2 NTAs in 0.1 M Na_2SO_4 under xenon lamp irradiation (0.3 V vs Ag/AgCl, 100 mW cm^{-2}).

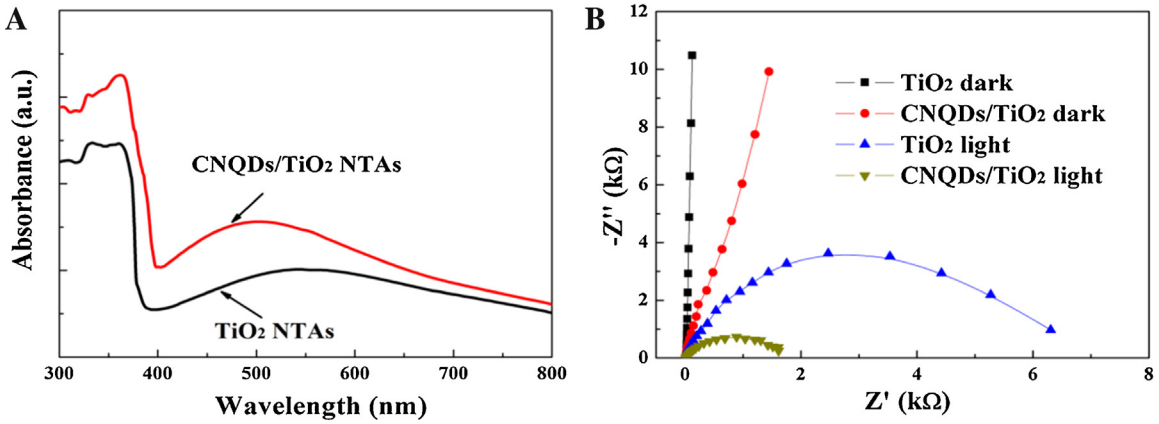

Fig. 6. (A) UV–vis absorption spectra and (B) EIS Nyquist plots of TiO_2 NTAs and CNQD/TiO_2 NTAs under dark and simulated solar light illumination (0 V vs Ag/AgCl, 100 mW cm^{-2}).

comparison (Fig. 7B). Only 18% and 51% RhB were removed over 90 min on CNQDs and TiO_2 NTAs, while more than 99% removal efficiency was achieved on CNQDs/TiO_2 NTAs. The kinetics constants (pseudo first order kinetics) of CNQDs/TiO_2 NTAs was calculated as 0.029 min^{-1}, which is 3.0 times and 16.1 times of those from pristine TiO_2 (0.0080 min^{-1}) and CNQDs (0.0018 min^{-1}). In addition, the PEC degradation of RhB was conducted under visible light illumination, as shown in Fig. S9A. Nearly no RhB was removed by TiO_2 NTAs after 240 min PEC reaction, however, more than 40% RhB was degraded by CNQDs/TiO_2 at the same conditions. The kinetic rate of CNQDs/TiO_2 for RhB removal (0.00234 min^{-1}) under visible light is about 14.9 times higher than that of pristine TiO_2 (0.000157 min^{-1}) (see Fig. S9B), revealing significantly improved visible-light activity after CNQDs modification.

Total organic carbon (TOC) measurements were carried out to measure the mineralization level during RhB degradation (Fig. S10). During the PEC process by CNQDs/TiO_2 NTAs, the RhB solution (10 mg L^{-1}) was totally decolorized after 90 min irradiation by CNQDs/TiO_2 NTAs and 54% of the TOC removal can be observed by CNQDs/TiO_2 NTAs with after 90 min irradiation, and TOC removal efficiency increased to 72% when the irradiation time was extended to 180 min. By contrast, TiO_2 NTAs displayed relatively limited TOC removal of 19.1% and 31.8% for 90 min and 180 min irradiation, respectively. These results indicate that RhB has been not only

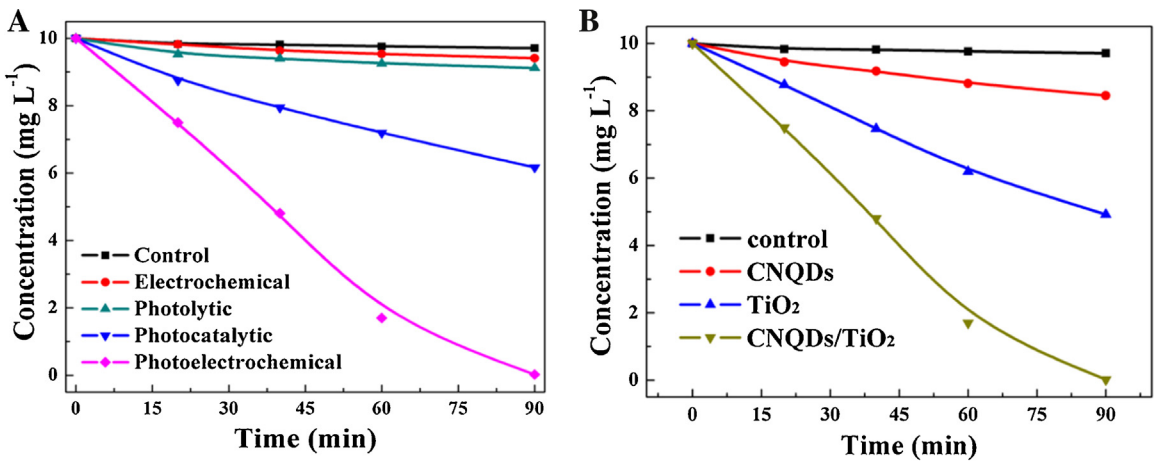

Fig. 7. (A) Degradation of RhB by different process using CNQDs/TiO_2 NTAs and (B) PEC degradation of RhB using CNQDs, TiO_2 and CNQDs/TiO_2 NTAs photoelectrodes (0.3 V vs Ag/AgCl, 100 mW cm^{-2}).

decolorized but also have potential to realize thorough mineralization by CNQDs/TiO_2. The de-ethylated products of RhB undergo significant decomposition upon further irradiation and that the cleavage of the whole conjugated chromosphore structure on the dyes occurs only to some extent by CNQDs/TiO_2 NTAs. Besides the PEC activity, the stability is another important factor for a photocatalyst during the PEC degradation process. The stability of CNQDs/TiO_2 NTA was tested by degrading RhB with one electrode for continuous 5 times under the same conditions (Fig. S11). During the 5 repeated PEC cycles, the RhB removal efficiency remained almost unchanged (99.8% for first run and 98.8% for the fifth run), indicating the good stability of CNQDs/TiO_2 NTAs when applied as a photoanode for RhB degradation, where the excellent pollutants removal efficiency was achieved as well.

The radicals and holes trapping experiments were designed to further elucidate the PEC degradation mechanism of RhB over CNQDs/TiO_2 NTAs. The effects of ethylene diamine tetra-acetic acid (EDTA, a typical hole scavenger), tert-butanol (t-BuOH, hydroxyl radicals quencher) and ascorbic acid (superoxide quencher) on the photodegradation efficiency of RhB in the presence of CNQDs/TiO_2 NTAs were investigated, and the results are shown in Fig. 8A. It can be seen clearly from the result that the PEC degradation of RhB was slightly retarded with about 71.3% RhB removal by the injection of a scavenger for holes (EDTA), which implied the minor role of holes either acting as the oxidizing agent or the origination of the hydroxyl radicals in this process. With the addition of tBuOH, an efficient hydroxyl radicals quencher, the degradation efficiency of RhB was depressed remarkably with only 29.8% of RhB degraded after 90 min, indicating hydroxyl radicals was the primary oxidant during the degradation process. In the presence of ascorbic acid (super oxide radicals scavenger), a moderate suppression about 54.3% removal of RhB was observed within 90 min. These results further confirm that hydroxyl radicals are the primary active species in this system, while superoxide radicals and holes are also involved.

To further verify the formation of active species involved in the PEC process, the ESR spin-trap technique (with DMPO) was employed to characterize the photo-generated reactive oxygen species over CNQDs/TiO_2 NTAs under solar light irradiation. The characteristic four peaks of DMPO—$OH^•$ with intensity 1:2:2:1 can be clearly observed in the ESR signal (Fig. 8B), and this is similar to spectra reported by other researchers [24,53,54], elucidating that $OH^•$ radicals were generated on the electrode under irradiation and no signals were observed in dark condition. Besides, it is well known that oxygen can easily trap an electron from the conduction band of TiO_2 forming superoxide. The formation of superoxide radicals were also examined by DMPO spin trapping ESR techniques in methanolic media. Fig. 8C displays the ESR spectrum of DMPO—O_2^- under light irradiation and the characteristics peaks can be observed in the CNQDs/TiO_2 NTAs electrode while no signals in the dark, showing that superoxide radicals were efficiently generated over CNQDs/TiO_2 under solar light. These results are in accordance with the previous radicals capture experiments.

Lastly, the stability of the CNQDs/TiO_2 phtoanode and their performance for water splitting were evaluated in a three-electrode configuration. It is notable that the photocurrent of pristine TiO_2 and CNQDs/TiO_2 are both very stable, nearly no decreases after 6000 s water splitting (Fig. 9A), implying the high stability of these nanotubular photoanodes. The hydrogen production rate over CNQDs//TiO_2 reached up to 22.0 μmol h^{-1} cm^{-2}, while the rate over pristine TiO_2 is only 7.1 μmol h^{-1} cm^{-2} (Fig. 9B). The results display that PEC water splitting to produce H_2 and O_2 was indeed occurred on CNQDs//TiO_2 photoanodes rather than other side reactions. These promising results demonstrate bright prospects to construct efficient photoanodes using earth-abundant elements for direct PEC water splitting systems.

Based on the above results, a possible charge transfer and separation mechanism of prepared CNQDs/TiO_2 photoanode is proposed in Fig. 10. Upon solar light irradiation, photo-generated holes and electrons are generated in the valence band (VB) and conduction band (CB) of TiO_2 and CNQDs, respectively. Due to the band alignment and potential difference, photo-generated electrons in CB of CNQDs can transfer easily to the CB of TiO_2, then they can go along vertical self-organized tubular structure to Ti substrate, realizing fast charge transfer and separation. The electrons ultimately transfer to the counter electrode to reduce water for production of hydrogen under the external electric field. Simultaneously, the generated holes at the VB of TiO_2 can efficiently inject to the VB of CNQDs. The accumulated holes in the VB of CNQDs will be consumed by oxidizing water to form oxygen. Thus, the photo-generated electron-hole pairs are effectively separated, thereby leading to the significantly enhanced PEC performance.

4. Conclusion

In summary, bifunctional molecules MPA was employed to modify TiO_2 NTAs by CNQDs to form an efficient heterojunction structure. The prepared CNQDs/TiO_2 NTAs Exhibit 350% enhanced and stable PEC response due to the remarkably enhanced visible light absorption and improved charge transfer and separation.

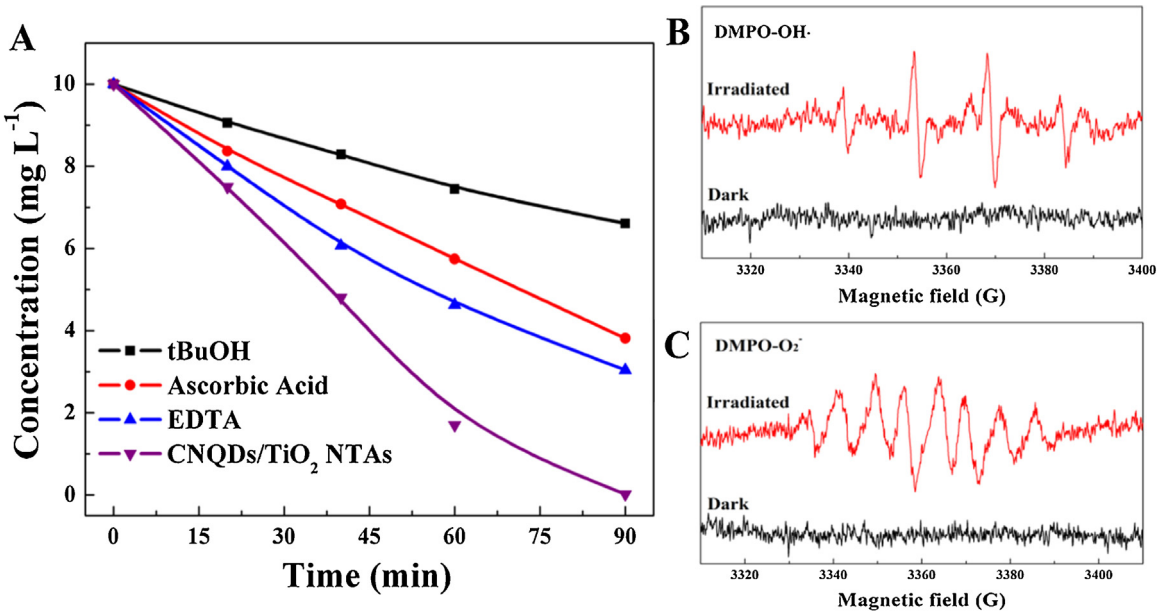

Fig. 8. (A) RhB removal efficiency using CNQDs/TiO_2 NTAs with various additives under simulated solar light illumination; DMPO spin-trapping ESR spectra recorded at ambient temperature (B) in aqueous dispersion (for DMPO—•OH) and (C) in methanol dispersion (for DMPO—O_2^-) at the presence of CNQDs/TiO_2 NTAs under light irradiation.

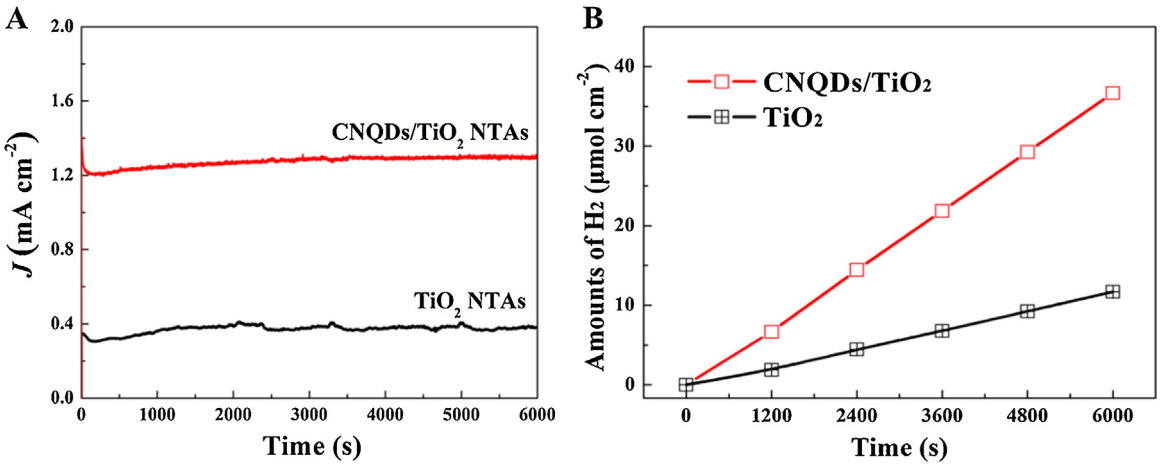

Fig. 9. (A) Stability test and (B) corresponding hydrogen evolution over CNQDs/TiO_2 photoanode in aqueous solution under simulated solar light illumination.

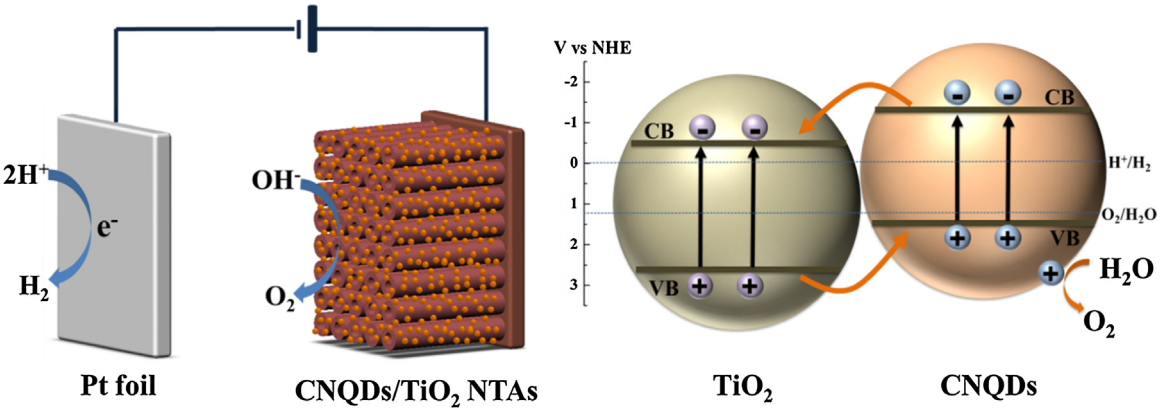

Fig. 10. Schematic energy band structure and proposed mechanism of charge transfer and separation of CNQDs/TiO_2 NTAs.

RhB was chosen as target to evaluate the PEC performance of prepared CNQDs/TiO_2 NTAs electrode, displaying remarkably enhanced removal efficiency than TiO_2 NTAs at the same condition. Also, the prepared sample was used as photoanode for direct PEC water splitting in neutral solution, giving a H_2 production rate of 22.0 μmol h^{-1} cm^{-2} at 0.3 V vs Ag/AgCl. The significant improve-

ment of PEC capability for the CNQDs/TiO_2 NTAs benefits from enhanced visible-light harvesting and reduced recombination of photo-generated electron–hole pairs due to the synergistic effect of heterojunction structure and organized morphology of TiO_2 NTAs.

Acknowledgement

The authors are grateful of the financial support from HK Research Grant Council under the grant number HKUST 622813.

Appendix A. Supplementary data

Supplementary data associated with this article can be found, in the online version, at http://dx.doi.org/10.1016/j.apcatb.2015.12.050.

References

[1] D.S. Bhatkhande, V.G. Pangarkar, A.A. Beenackers, J. Chem. Technol. Biotechnol. 77 (2002) 102–116.
[2] M. Grätzel, Nature 414 (2001) 338–344.
[3] X. Chen, S. Shen, L. Guo, S.S. Mao, Chem. Rev. 110 (2010) 6503–6570.
[4] M.G. Walter, E.L. Warren, J.R. McKone, S.W. Boettcher, Q. Mi, E.A. Santori, N.S. Lewis, Chem. Rev. 110 (2010) 6446–6473.
[5] X. Chen, S.S. Mao, Chem. Rev. 107 (2007) 2891–2959.
[6] J. Su, H. Yu, X. Quan, S. Chen, H. Wang, Appl. Catal. B: Environ. 138 (2013) 427–433.
[7] J. Su, H. Yu, S. Chen, X. Quan, Q. Zhao, Sep. Purif. Technol. 96 (2012) 154–160.
[8] T.L. Thompson, J.T. Yates, Chem. Rev. 106 (2006) 4428–4453.
[9] Y. Ma, X. Wang, Y. Jia, X. Chen, H. Han, C. Li, Chem. Rev. 114 (2014) 9987–10043.
[10] K. Lee, A. Mazare, P. Schmuki, Chem. Rev. 114 (2014) 9385–9454.
[11] P. Roy, S. Berger, P. Schmuki, Angew. Chem. Int. Ed. 50 (2011) 2904–2939.
[12] X. Quan, S. Yang, X. Ruan, H. Zhao, Environ. Sci. Technol. 39 (2005) 3770–3775.
[13] G.K. Mor, K. Shankar, M. Paulose, O.K. Varghese, C.A. Grimes, Nano Lett. 5 (2005) 191–195.
[14] P. Geng, J. Su, C. Miles, C. Comninellis, G. Chen, Electrochim. Acta 153 (2015) 316–324.
[15] O.K. Varghese, C.A. Grimes, Sol. Energy Mater. Sol. Cells 92 (2008) 374–384.
[16] N. Lu, X. Quan, J. Li, S. Chen, H. Yu, G. Chen, J. Phys. Chem. C 111 (2007) 11836–11842.
[17] Y.K. Lai, J.Y. Huang, H.F. Zhang, V.P. Subramaniam, Y.X. Tang, D.G. Gong, L. Sundar, L. Sun, Z. Chen, C.J. Lin, J. Hazard. Mater. 184 (2010) 855–863.
[18] C. Das, P. Roy, M. Yang, H. Jha, P. Schmuki, Nanoscale 3 (2011) 3094–3096.
[19] T.M. Suzuki, G. Kitahara, T. Arai, Y. Matsuoka, T. Morikawa, Chem. Commun. 50 (2014) 7614–7616.
[20] S.K. Mohapatra, N. Kondamudi, S. Banerjee, M. Misra, Langmuir 24 (2008) 11276–11281.
[21] Z. Zhang, L. Zhang, M.N. Hedhili, H. Zhang, P. Wang, Nano Lett. 13 (2013) 14–20.
[22] H. Zhang, X. Quan, S. Chen, H. Yu, N. Ma, Chem. Mater. 21 (2009) 3090–3095.
[23] J. Zhang, J.H. Bang, C. Tang, P.V. Kamat, ACS Nano 4 (2009) 387–395.
[24] J. Su, P. Geng, X. Li, Q. Zhao, X. Quan, G. Chen, Nanoscale 7 (2015) 16282–16289.
[25] G. Li, L. Wu, F. Li, P. Xu, D. Zhang, H. Li, Nanoscale 5 (2013) 2118–2125.
[26] W.-T. Sun, Y. Yu, H.-Y. Pan, X.-F. Gao, Q. Chen, L.-M. Peng, J. Am. Chem. Soc. 130 (2008) 1124–1125.
[27] A. Kongkanand, K. Tvrdy, K. Takechi, M. Kuno, P.V. Kamat, J. Am. Chem. Soc. 130 (2008) 4007–4015.
[28] H. Yang, W. Fan, A. Vaneski, A.S. Susha, W.Y. Teoh, A.L. Rogach, Adv. Funct. Mater. 22 (2012) 2821–2829.
[29] C. Ratanatawanate, C. Xiong, K.J. Balkus Jr., ACS Nano 2 (2008) 1682–1688.
[30] Z.-X. Li, Y.-L. Xie, H. Xu, T.-M. Wang, Z.-G. Xu, H.-L. Zhang, J. Photochem. Photobiol. A: Chem. 224 (2011) 25–30.
[31] X. Wang, K. Maeda, A. Thomas, K. Takanabe, G. Xin, J.M. Carlsson, K. Domen, M. Antonietti, Nat. Mater. 8 (2009) 76–80.
[32] J. Zhang, X. Chen, K. Takanabe, K. Maeda, K. Domen, J.D. Epping, X. Fu, M. Antonietti, X. Wang, Angew. Chem. Int. Ed. 49 (2010) 441–444.
[33] K. Maeda, X. Wang, Y. Nishihara, D. Lu, M. Antonietti, K. Domen, J. Phys. Chem. C 113 (2009) 4940–4947.
[34] Y. Wang, Y. Di, M. Antonietti, H. Li, X. Chen, X. Wang, Chem. Mater. 22 (2010) 5119–5121.
[35] S.C. Yan, Z.S. Li, Z.G. Zou, Langmuir 25 (2009) 10397–10401.
[36] C. Pan, J. Xu, Y. Wang, D. Li, Y. Zhu, Adv. Funct. Mater. 22 (2012) 1518–1524.
[37] S. Yang, X. Feng, X. Wang, K. Mullen, Angew. Chem. Int. Ed. 50 (2011) 5339–5343.
[38] T.Y. Ma, S. Dai, M. Jaroniec, S.Z. Qiao, Angew. Chem. Int. Ed. 53 (2014) 7281–7285.
[39] X. Zhang, X. Xie, H. Wang, J. Zhang, B. Pan, Y. Xie, J. Am. Chem. Soc. 135 (2013) 18–21.
[40] J. Zhou, Y. Yang, C.-Y. Zhang, Chem. Commun. 49 (2013) 8605–8607.
[41] I. Robel, V. Subramanian, M. Kuno, P.V. Kamat, J. Am. Chem. Soc. 128 (2006) 2385–2393.
[42] Y. Zhang, T. Mori, L. Niu, J. Ye, Energy Environ. Sci. 4 (2011) 4517–4521.
[43] Z. Zhang, K. Leinenweber, M. Bauer, L.A. Garvie, P.F. McMillan, G.H. Wolf, J. Am. Chem. Soc. 123 (2001) 7788–7796.
[44] S. Barman, M. Sadhukhan, J. Mater. Chem. 22 (2012) 21832–21837.
[45] J. Sun, J. Zhang, M. Zhang, M. Antonietti, X. Fu, X. Wang, Nat. Commun. (2012) 1139.
[46] Y. Hou, X. Li, Q. Zhao, X. Quan, G. Chen, J. Mater. Chem. 21 (2011) 18067–18076.
[47] W. Wang, C.Y. Jimmy, Z. Shen, D.K. Chan, T. Gu, Chem. Commun. 50 (2014) 10148–10150.
[48] S. Ray, A. Saha, N.R. Jana, R. Sarkar, J. Phys. Chem. C 113 (2009) 18546–18551.
[49] S. Liu, J. Tian, L. Wang, Y. Zhang, X. Qin, Y. Luo, A.M. Asiri, A.O. Al-Youbi, X. Sun, Adv. Mater. 24 (2012) 2037–2041.
[50] S. Martha, A. Nashim, K.M. Parida, J. Mater. Chem. A 1 (2013) 7816–7824.
[51] J. Fu, B. Chang, Y. Tian, F. Xi, X. Dong, J. Mater. Chem. A 1 (2013) 3083–3090.
[52] K. Schwinghammer, B. Tuffy, M.B. Mesch, E. Wirnhier, C. Martineau, F. Taulelle, W. Schnick, J. Senker, B.V. Lotsch, Angew. Chem. Int. Ed. 52 (2013) 2435–2439.
[53] Y. Lu, H. Yu, S. Chen, X. Quan, H. Zhao, Environ. Sci. Technol. 46 (2012) 1724–1730.
[54] Y. Hou, X. Li, Q. Zhao, G. Chen, C.L. Raston, Environ. Sci. Technol. 46 (2012) 4042–4050.